Bioorganic & Medicinal Chemistry 21 (2013) 3873–3881

Contents lists available at SciVerse ScienceDirect

Bioorganic & Medicinal Chemistry

journal homepage: www.elsevier.com/locate/bmc

Novel 1*H*-imidazol-2-amine derivatives as potent and orally active vascular adhesion protein-1 (VAP-1) inhibitors for diabetic macular edema treatment

Takayuki Inoue [a,*], Masataka Morita [a], Takashi Tojo [a], Akira Nagashima [a], Ayako Moritomo [a], Hiroshi Miyake [b]

[a] Drug Discovery Research, Astellas Pharma Inc., 21 Miyukigaoka, Tsukuba, Ibaraki 305-8585, Japan
[b] Astellas Research Technology Co., Ltd, 21 Miyukigaoka, Tsukuba, Ibaraki 305-8585, Japan

ARTICLE INFO

Article history:
Received 14 March 2013
Revised 2 April 2013
Accepted 4 April 2013
Available online 19 April 2013

Keywords:
Vascular adhesion protein-1
Inhibitor
Macular edema
Guanidine bioisostere
1*H*-Imidazol-2-amine derivative

ABSTRACT

Novel thiazole derivatives were synthesized and evaluated as vascular adhesion protein-1 (VAP-1) inhibitors. Although we previously identified a compound (**2**) with potent VAP-1 inhibitory activity in rats, the human activity was relatively weak. Here, to improve the human VAP-1 inhibitory activity of compound **2**, we first evaluated the structure–activity relationships of guanidine bioisosteres as simple small molecules and identified a 1*H*-benzimidazol-2-amine (**5**) with potent activity compared to phenylguanidine (**1**). Based on the structure of compound **5**, we synthesized a highly potent VAP-1 inhibitor (**37b**; human IC_{50} = 0.019 μM, rat IC_{50} = 0.0051 μM). Orally administered compound **37b** also markedly inhibited ocular permeability in streptozotocin-induced diabetic rats after oral administration, suggesting it is a promising compound for the treatment of diabetic macular edema.

1. Introduction

Vascular adhesion protein-1 (VAP-1) is an endothelial surface glycoprotein with homology to semicarbazide-sensitive amine oxidases. Two types of VAP-1 have been identified: a membrane-binding type present in vascular endothelium and a soluble type found in serum. Membrane-bound VAP-1 adheres to white blood cells and lymphocytes and is involved in inflammation,[1] whereas the soluble form displays amine oxidase activity that is involved in amine detoxification.

VAP-1 is highly expressed in vascular endothelial cells within inflamed areas and is responsible for the metabolism of primary amines, such as methylamine and aminoacetone,[2,3] and leukocyte trafficking. VAP-1 catalyzes the oxidative deamination of primary amines to produce the corresponding aldehydes, in addition to the cytotoxic reaction products ammonia and hydrogen peroxide,[4] which may be associated with a number of vasculopathies.[5,6] Consistent with these properties, an increase in plasma and membrane-associated VAP-1 derived from adipocytes and vascular tissue has been observed in many inflammation-associated diseases.[7] VAP-1 was recently reported to be expressed on retinal vascular endothelial cells, where it functions in leukocyte recruitment on retinal vessels.[8] The accumulation of toxic by-products and increased leukocyte adhesion activity are indicative of the breakdown of the blood–retinal barrier and are thought to lead to the severe macular edema that is often seen in diabetic retinopathy, which is the leading cause of blindness in humans. Even minimal disruption of the macular region due to edema can cause severe visual loss, and if left untreated, can lead to irreversible changes in the macular region and the exacerbation of retinopathy.

We recently described a novel VAP-1 inhibitor, compound **2**, which was synthesized from a high-throughput screening (HTS) hit compound.[9] However, compound **2** showed approximately 16-fold lower VAP-1 inhibitory activity in humans than in rats (human IC_{50}, 0.23 μM; rat IC_{50}, 0.014 μM). Therefore, to improve the human VAP-1 inhibitory activity of compound **2**, here, we attempted to further modify the phenylguanidine moiety, which was previously identified as being critical for human VAP-1 inhibitory activity based on the results of a docking study between compound **2** and human VAP-1 enzyme.[9] We initially attempted to identify bioisosteres of phenylguanidine (**1**) with human VAP-1 inhibitory activity using the design strategy shown in Figure 1. Additionally, we conducted optimization of the phenylguanidine bioisostere, 1*H*-benzimidazol-2-amine (**5**), and introduced the

* Corresponding author. Tel.: +81 29 829 6227; fax: +81 29 854 1519.
E-mail address: takayuki.inoue@astellas.com (T. Inoue).

0968-0896
http://dx.doi.org/10.1016/j.bmc.2013.04.011

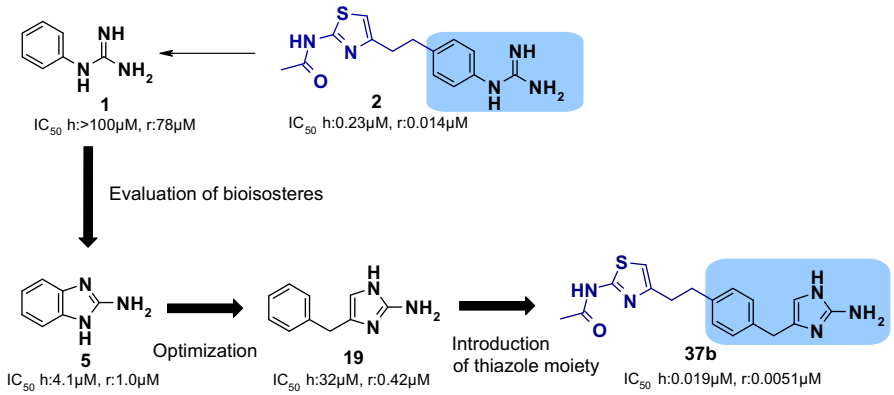

Figure 1. Summary for synthesizing bioisosteres of phenylguanidine.

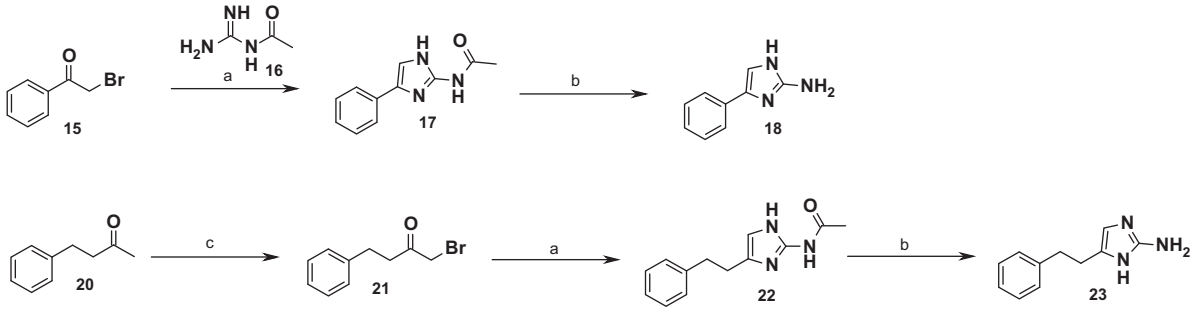

Scheme 1. Reagents and conditions: (a) compound **16**, DMF; (b) 6 M HCl, MeOH, reflux; (c) (1) Br_2, HBr, AcOH, (2) acetone.

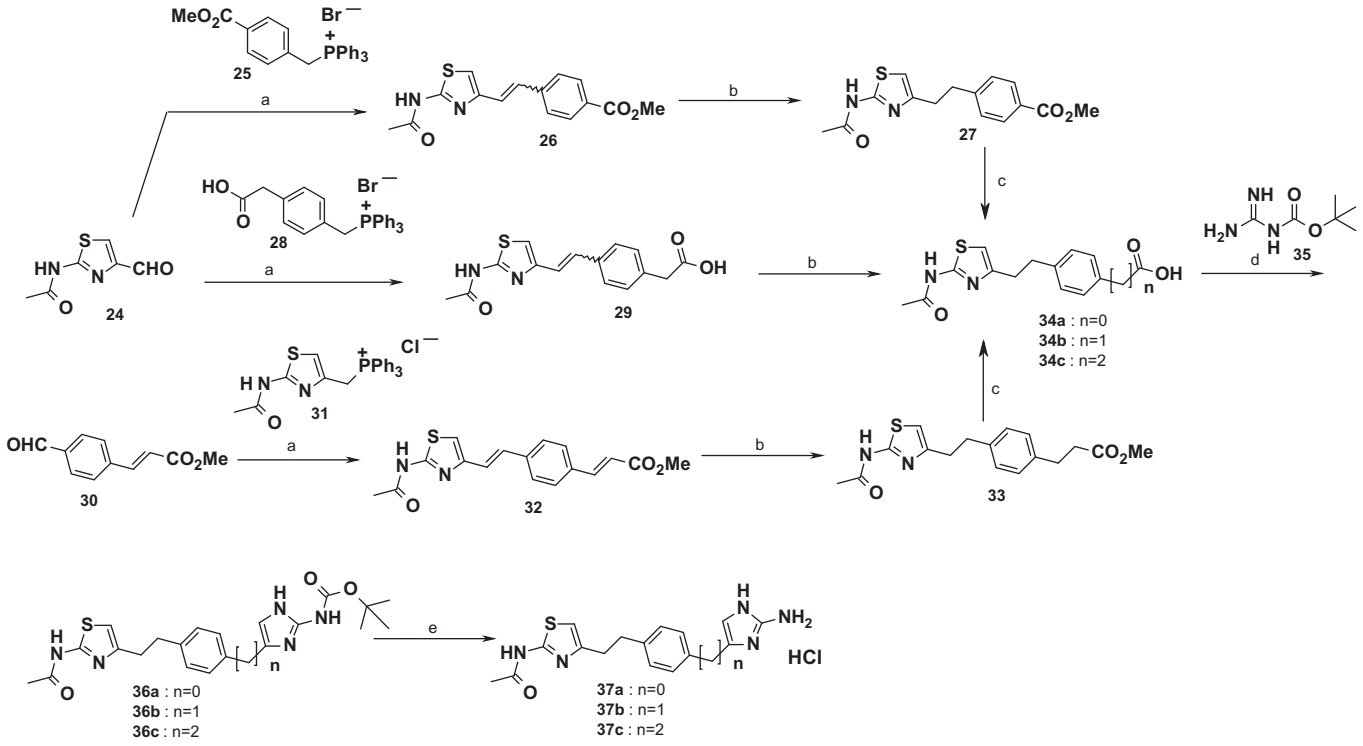

Scheme 2. Reagents and conditions: (a) compounds **25** or **28** or **31**, ^{t}BuOK, DMF; (b) H_2 (3 atm), 10% Pd–C, AcOH, MeOH, THF; (c) 1 M NaOH, EtOH, reflux; (d) (1) $(COCl)_2$, CH_2Cl_2, DMF, (2) $TMSCH_2N_2$, CH_2Cl_2, (3) 4 M HCl/AcOEt, CH_2Cl_2/DMF, (4) compound **35**, DMF; (e) 4 M HCl/AcOEt, MeOH.

thiazole pharmacophore of compound **2** to the obtained 4-benzyl-1*H*-imidazol-2-amine (**19**). Consequently, we succeeded in synthesizing compound **37b**, which displayed strong inhibitory activities against both human and rat VAP-1.

In this paper, we discuss the synthesis and structure–activity relationships (SARs) of this series of novel 1*H*-imidazol-2-amine derivatives as candidate human VAP-1 inhibitors.

2. Chemistry

The synthesis of 1*H*-imidazol-2-amine derivatives **18** and **23** is shown in Scheme 1. Cyclization of 2-bromo-1-phenylethanone (**15**) with *N*-carbamimidoylacetamide (**16**) gave *N*-(4-phenyl-1*H*-imidazol-2-yl)acetamide (**17**). Deprotection of the acetyl group in compound **17** with 6 M hydrogen chloride in refluxing methanol gave 4-phenyl-1*H*-imidazol-2-amine (**18**). Bromination of 4-phenylbutan-2-one (**20**) with bromine gave 1-bromo-4-phenylbutan-2-one (**21**). 4-(2-Phenylethyl)-1*H*-imidazol-2-amine (**23**) was obtained from **21** by the same procedure as that used for compound **18**.

Scheme 2 shows the syntheses of compounds **37a–c**. The Wittig reaction of aldehyde derivatives **24** and **30** with the corresponding phosphonium salts **25**, **28**, and **31** and subsequent hydrogenation in the presence of palladium on carbon gave intermediates **27**, **33**, and **34b**. Hydrolysis of ester derivatives **27** and **33** with 1 M sodium hydroxide in refluxing ethanol gave the corresponding carboxylic acid derivatives **34a**,**c**.

Treatment of **34a–c** with oxalyl chloride followed by ketonization with (trimethylsilyl)diazomethane, substitution of the trimethylsilyl group with chloride, and cyclization with *tert*-butyl carbamimidoylcarbamate (**35**) provided **36a–c**, respectively. The deprotection of the *tert*-butoxycarbonyl (Boc) group of **36a–c** afforded the desired compounds **37a–c**.

3. Results and discussion

The compounds were evaluated for in vitro VAP-1 inhibitory activity against human and rat VAP-1. VAP-1 activities were determined using a radiochemical enzyme assay with ^{14}C-benzylamine as an artificial substrate. The VAP-1 enzymes used in the assays were prepared from Chinese hamster ovary (CHO) cells stably expressing human or rat VAP-1.

We previously demonstrated that the guanidine moiety of compound **2** forms tight hydrogen bonds network with Asp386, but can also bind covalently to the trihydroxyphenylalanine quinone (TPQ) 471, indicating that the guanidine moiety is important for the VAP-1 inhibitor activity.[9] Here, we therefore focused on the synthesis of compounds with close structural similarity to phenylguanidine, such as imidazoline derivatives (**3**, **4**), 1*H*-benzimidazol-2-amine (**5**), and quinazolin-2-amine (**6**). The VAP-1 inhibitory activities of compounds **3–6** are shown in Table 1. Imidazoline derivatives **3** and **4**, and quinazolin-2-amine (**6**) showed no inhibitory activity, whereas 1*H*-benzimidazol-2-amine (**5**) exhibited strong VAP-1 inhibitory activity.

We next attempted to optimize the inhibitory activity of compound **5** (Table 2). Thiazole derivative **7** had no detectable VAP-1 inhibitory activity, suggesting that the NH of the imidazole moiety is required for the activity. 1*H*-Indol-2-amine (**8**) also exhibited a marked reduction in inhibitory activity compared to **5**, implying that the guanidine moiety is essential for VAP-1 inhibition. Deamination of **5** was also deleterious to the inhibitory activity (**9**), a result that is consistent with the fact that a primary amine-forming Schiff base is essential for the VAP-1 inhibitory activity of **5**.[9,13,14] Aminomethyl analogue **10** also lost the inhibitory activity, suggesting that the introduction of a methylene group increased the size of the guanidine moiety, thereby preventing the interaction of **10** with VAP-1. As the deletion of the benzene ring (**11**) also resulted in a significant reduction in VAP-1 inhibition, the benzene ring ap-

Table 1
VAP-1 inhibitory activities of phenylguanidine bioisosteres

Compd	Structure	VAP-1 Human[a]	VAP-1 Rat[b]
1[c]	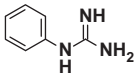	>100	78
3[d,c]	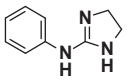	>100	>100
4[e,c]	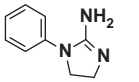	>100	>100
5[c]	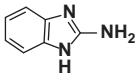	4.1	1.0
6[c]	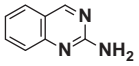	>100	>100

[a] IC_{50} data for human VAP-1 in μM ($n = 2$).
[b] IC_{50} data for rat VAP-1 in μM ($n = 2$).
[c] Commercially available.
[d] Hydrochloride salt.
[e] Hydrobromide salt.

Table 2
VAP-1 inhibitory activities of 1*H*-benzimidazol-2-amine derivatives

Compd	Structure	VAP-1 Human[a]	VAP-1 Rat[b]
5[c]	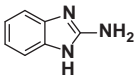	4.1	1.0
7[c]	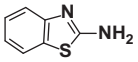	>100	>100
8[d,c]	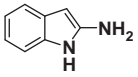	74	63
9[c]		>100	>100
10[e,c]	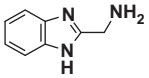	>100	>100
11[f,c]	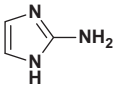	>100	90
12[c]	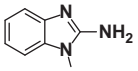	>100	80
13[c]	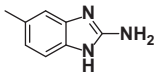	>100	9.3
14[c]	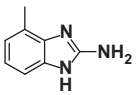	>100	1.0

[a] IC_{50} data for human VAP-1 in μM ($n = 2$).
[b] IC_{50} data for rat VAP-1 in μM ($n = 2$).
[c] Commercially available.
[d] Hydrochloride salt.
[e] Dihydrochloride salts.
[f] Hemisulfate salt.

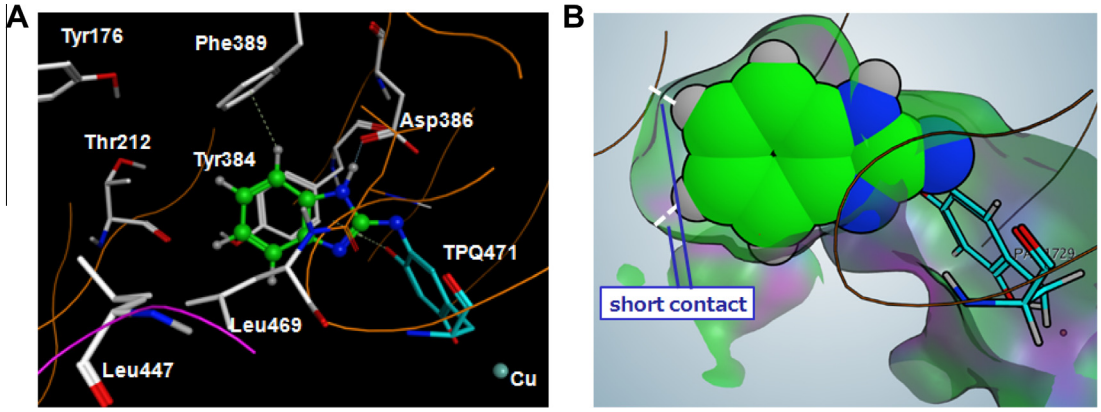

Figure 2. Computational docking results for compound **5** with human VAP-1. (A) Best docking solution (lowest binding energy) calculated by GOLD *ver.5.1.* for compound **5** (ball and stick representation; compound is colored blue for nitrogen and green for carbon) surrounded by the human VAP-1 active site. Key receptor residues are indicated. (B) Results of the docking analysis represented as an Active LP image (green, hydrophobic regions of the surface; blue, mildly polar regions; and purple, hydrogen-bonding regions).

Table 3
VAP-1 inhibitory activities of 1*H*-imidazol-2-amine derivatives

Compd	Structure	VAP-1 Human[a]	VAP-1 Rat[b]
5[c]	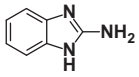	4.1	1.0
18	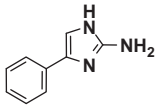	>100	44
19[c]	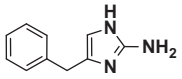	32	0.42
23	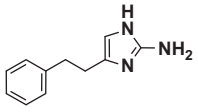	>100	4.8
37a[d]	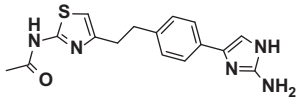	13	0.15
37b[d]	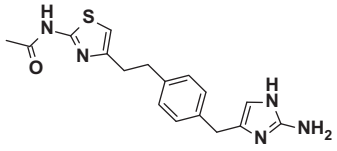	0.019	0.0051
37c[d]	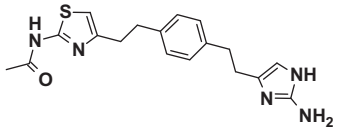	2.2	0.018

[a] IC_{50} data for human VAP-1 in μM ($n = 2$).
[b] IC_{50} data for rat VAP-1 in μM ($n = 2$).
[c] Commercially available.
[d] Hydrochloride salt.

pears necessary for activity. Among the examined derivatives, 1*H*-benzimidazol-2-amine (**5**) showed the most potent inhibitory activity against human and rat VAP-1. Subsequently, we introduced a methyl group at the 1, 4, or 5 position of 1*H*-benzimidazole-2-amine to determine the appropriate position to attach the thiazole moiety of the other main pharmacophore found in compound **2**. Unfortunately, all of the generated compounds (**12**–**14**) had no inhibitory activity against human VAP-1.

To understand the SAR of 1*H*-benzimidazole-2-amine, we examined compound **5** using a human VAP-1 docking model[9–14] with the GOLD program (version 5.1; Fig. 2). As an initial docking structure, the amine group at the 2-position of **5** formed a Schiff base intermediate with the TPQ moiety of VAP-1. In addition to the covalent interaction of the primary amine, the modeling also suggested that the NH of the imidazole ring of **5** formed a hydrogen bond with Asp386, the imidazole ring formed a π–proton interaction with TPQ471 (–OH), the benzene ring formed a π–π interaction with Tyr384, and the CH of the benzene ring formed a proton–π interaction with Phe389. We considered that even compact molecules such as **5** could exert potent inhibitory activity due to these five types of intermolecular interactions. In addition, as compound **5** just fit in the active center pocket of VAP-1, the introduction of additional substituents would likely block entry of the compound into the active site. These results were in approximate agreement with the SAR findings. Consequently, we considered that it was impossible to add any substituents into the benzimidazole moiety. Therefore, we searched for other bioisosteres of 1*H*-benzimidazol-2-amine with human VAP-1 inhibitory activity.

Based on the high potency of 1*H*-benzimidazol-2-amine (**5**), we examined whether spatial room could be generated by introducing flexibility between the phenyl and imidazole rings. First, optimization of the distance between the phenyl and imidazole rings of **5** was conducted by examining compounds with different linkers (Table 3). Among the examined compounds (**18**, **19**, and **23**), compound **19**, which contained a methylene linker between the phenyl and imidazole rings, showed the strongest inhibitory activity against human VAP-1. Compound **18**, which did not have a linker, and **23**, which contained an ethylene linker, had no detectable human VAP-1 inhibitory activity.

The results of the docking analysis of **19** with human VAP-1 are shown in Figure 3. The analysis indicated that the NH of the imidazole ring formed a hydrogen bond with Asn470, the imidazole ring formed a π–π interaction with Tyr384, and the benzene ring formed a π–proton interaction with Leu469. Compound **19** showed approximately 8-fold less potent human VAP-1 inhibitory activity compared to **5**, suggesting that the benzene ring of compound **19** is slightly exposed from the VAP-1 binding pocket due to the presence of a methylene moiety between the phenyl and imidazole rings, resulting in reduced affinity for VAP-1. However, we predicted that introducing a substituent at the 4-position of the benzene ring would be possible because this position faces toward the

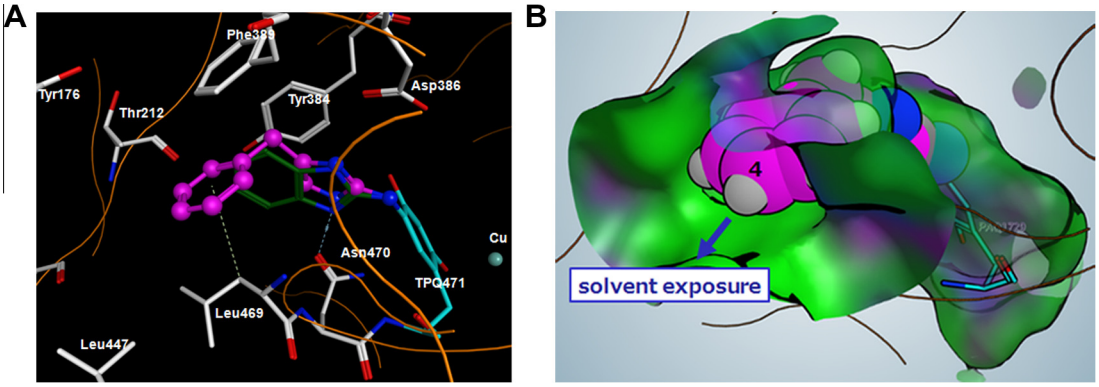

Figure 3. Computational docking results for compounds **5** and **19** with human VAP-1. (A) Best docking solution (lowest binding energy) calculated by GOLD *ver.5.1.* for compounds **5** (stick representation; compound is colored blue for nitrogen and green for carbon) and **19** (ball and stick representation; compound is colored blue for nitrogen and pink for carbon) surrounded by the human VAP-1 active site. Key receptor residues are indicated. (B) Results of the docking analysis represented as an Active LP image (green, hydrophobic surface regions; blue, mildly polar regions; and purple, hydrogen-bonding regions).

solvent side. Compound **19** showed greater than 3- and 186-fold improvements in human and rat VAP-1 inhibitory activities, respectively, compared to **1**. Therefore, we decided to introduce a thiazole moiety into compound **19**, generating compound **37b**. Compound **37b** showed satisfactory potency against both human and rat VAP-1 (Table 3), and had 12-fold higher inhibitory activity against human VAP-1 than **2**. Although compounds **18** and **23** had no detectable human VAP-1 inhibitory activity, we synthesized their thiazole derivatives (**37a** and **37c**) for confirmation. Consistent with the SAR results, both compounds exhibited lower potency compared to **37b**.

The results of the docking analysis of **37b** with human VAP-1 are shown in Figure 4. As expected, the amidothiazole moiety interacted with the active site of human VAP-1 enzyme. Specifically, the thiazole ring of **37b** formed π–proton interactions with Thr212 and Leu447, the sulfur atom in the thiazole ring made an S–O interaction[9,15] with the Thr210 backbone carbonyl oxygen, the amide moiety formed a proton–π interaction with Tyr176, and the acetyl moiety formed a CH–O interaction with Asp180. Together, these analysis results suggest that strong interactions between the amidothiazole moiety and human VAP-1 enzyme led to the increased inhibitory activity of **37b** compared to **2**. In particular, we speculate that **37b** is more potent than **2** due to the following two reasons: first, the anchor-part substructure of **37b** (**19**: IC_{50} = 32 μM) is more potent than that of **2** (**1**: IC_{50} = >100 μM) and second, the thiazole moiety of **37b** is positioned optimally in the active site of VAP-1, resulting three times as many interactions with the enzyme as **2** (Fig. 4).

The inhibitory properties of **37b** were further compared against other amine oxidases (AOs), including human monoamine oxidase (MAO)-A and -B, using a fluorometric enzymatic assay (Table 4). Compound **37b** displayed greater than 580-fold selectivity for VAP-1 inhibitory activity over MAO-A/B. We also examined the inhibitory effect of **37b** on plasma VAP-1 activity in streptozotocin (STZ)-induced diabetic rats (Fig. 5A).[9] Significant inhibitory activity was observed at a dose of 10 mg/kg after oral (po) administration.

Table 4
Selectivity of compounds **2** and **37b** for VAP-1 and MAO-A,B

Compd	VAP-1 Human IC_{50} (μM)[b]	VAP-1 Rat IC_{50} (μM)[b]	MAO[a]-A Human IC_{50} (μM)[b]	MAO[a]-B Human IC_{50} (μM)[b]
2	0.23	0.014	>100	60
37b	0.019	0.0051	>100	11

[a] MAO, monoamine oxidase.
[b] $n = 2$.

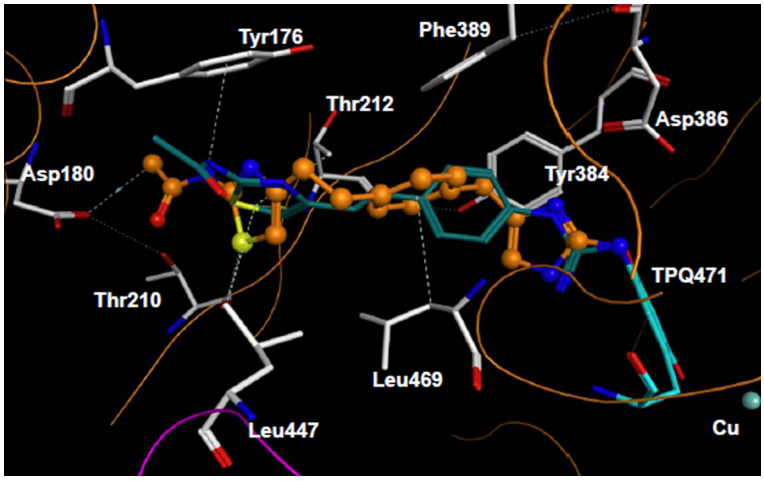

Figure 4. Computational docking results for compounds **2** and **37b** with human VAP-1. Best docking solution (lowest binding energy) calculated by GOLD *ver.5.1.* for compounds **2** (stick representation; compound is colored blue for nitrogen, red for oxygen, yellow for sulfur, and cyan for carbon) and **37b** (ball and stick representation; compound is colored blue for nitrogen, red for oxygen, yellow for sulfur, and orange for carbon) surrounded by the human VAP-1 active site. Key receptor residues are indicated.

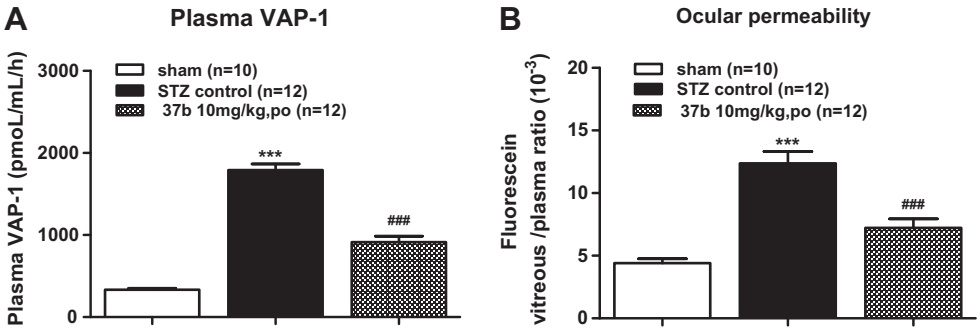

Figure 5. Pharmacodynamic profile and pharmacology of compound **37b** in rats. (A) Inhibitory effect on plasma VAP-1 activity in streptozotocin (STZ)-induced diabetic rats (n = 10–12, 10 mg/kg, po) at 2 weeks after treatment with compound **37b**. The plasma VAP-1 activity was measured using a radiolabeled enzyme assay with ^{14}C-benzylamine as the substrate. (B) Effect of compound **37b** (n = 10–12, 10 mg/kg, po) on ocular permeability in STZ-induced diabetic rats. $^{***}P$ <0.001 and $^{\#\#\#}P$ <0.001, Student's t-test versus sham and STZ control groups, respectively. Error bars indicate standard error.

Finally, we evaluated the effect of **37b** on ocular permeability in STZ-induced diabetic rats as a pathological model of macular edema (Fig. 5B). The oral administration of **37b** at 10 mg/kg had an inhibitory effect on ocular permeability, suggesting that **37b** is a promising compound for the treatment of diabetic macular edema.

4. Conclusion

We have developed a 1*H*-imidazol-2-amine derivative with an acetamidothiazole moiety that functions as a novel orally active VAP-1 inhibitor. The compound, **37b**, which was synthesized based on the evaluation and optimization of guanidine bioisosteres, is the most potent VAP-1 inhibitor reported to date and has excellent selectivity for VAP-1 compared to other AOs. Furthermore, orally administered **37b** was effective in a pathological model of macular edema, suggesting it is a promising compound for the treatment of diabetic macular edema.

5. Experimental

5.1. Chemistry

^{1}H NMR spectra were measured with a JEOL EX400 or GX500 spectrometer. Chemical shifts are expressed in δ units using tetramethylsilane as the standard (in the NMR description, s, singlet; d, doublet; t, triplet; q, quartet; m, multiplet; and br, broad peak). Mass spectra were recorded with Hitachi M-80 or JEOL JMS-DX300 spectrometers. Silica gel column chromatography was performed using Wakogel C-200 or Merck Silica Gel 60. Unless otherwise noted, all commercial reagents and solvents were used without further purification.

The following compounds were purchased from commercial sources and used without further purification: **1** (2002-16-6), **3** (1848-75-5), **4** (41213-54-1), **5** (934-32-7), **6** (1687-51-0), **7** (136-95-8), **8** (27878-37-1), **9** (51-17-2), **10** (5993-91-9), **11** (1450-93-7), **12** (1622-57-7), **13** (6285-68-3), **14** (171082-91-0), and **19** (862281-44-5).

5.1.1. *N*-(4-Phenyl-1*H*-imidazol-2-yl)acetamide (17)

A solution of 2-bromo-1-phenylethanone (**15**) (1.0 g) in DMF (20 mL) was added to a solution of *N*-carbamimidoylacetamide (**16**) (1.0 g) at 0 °C. The reaction mixture was stirred at room temperature for 15 h and then concentrated in vacuo. The obtained solid was washed with CH_3CN to give **17** (546 mg, 54%) as an off-white solid. ^{1}H NMR (DMSO-d_6) δ 2.07 (3H, s), 7.16 (1H, t, J = 7.5 Hz), 7.25 (1H, s), 7.32 (2H, t, J = 7.5 Hz), 7.71 (2H, d, J = 7.5 Hz), 11.22 (1H, s), 11.61 (1H, br s); FAB MS m/e (M+H)$^+$ 202; HRMS (ESI) Calcd for $C_{11}H_{12}N_3O$ (M+H)$^+$: 202.0980, found: 202.0986.

5.1.2. 4-Phenyl-1*H*-imidazol-2-amine (18)

A mixture of **17** (500 mg), 6 M HCl (2.2 mL), and MeOH (2.5 mL) was refluxed for 3 h. After cooling the mixture to room temperature, the precipitate was filtered off and the filtrate was then concentrated in vacuo. The obtained residue was dissolved in H_2O and the resulting solution was neutralized with 1 M NaOH. The precipitate was collected in vacuo and then washed with H_2O and Et_2O to give **18** (131 mg, 33%) as a pale brown solid. ^{1}H NMR (DMSO-d_6) δ 5.25 (2H, s), 6.96 (1H, s), 7.07 (1H, t, J = 7.5 Hz), 7.26 (2H, t, J = 7.5 Hz), 7.57 (2H, d, J = 7.5 Hz), 10.53 (1H, br s); FAB MS m/e (M+H)$^+$ 160; HRMS (ESI) Calcd for $C_9H_{10}N_3$ (M+H)$^+$: 160.0875, found: 160.0871; Anal. Calcd for $C_9H_9N_3{\cdot}0.3H_2O$: C, 65.68; H, 5.88; N, 25.53. Found: C, 65.81; H, 5.49; N, 25.19.

5.1.3. 1-Bromo-4-phenylbutan-2-one (21)

To a solution of 4-phenylbutan-2-one (**20**) (3.0 g) in AcOH (7 mL) and 48% aqueous HBr (3 mL) was added a solution of Br_2 (6.5 g) in AcOH (5 mL) at 0 °C. After stirring the reaction mixture at room temperature for 4 h, acetone (30 mL) was added to the solution, and the reaction mixture was further stirred at room temperature for 14 h. The mixture was then concentrated in vacuo, diluted with brine, and extracted twice with CH_2Cl_2. The combined organic layer was dried over anhydrous $MgSO_4$, and then evaporated in vacuo. The obtained residue was purified by flash column chromatography over silica gel with hexane/AcOEt (40:1–10:1) as an eluent to give **21** (1.5 g, 34%) as a pale brown oil. CI MS m/e (M)$^+$ 227.

5.1.4. *N*-[4-(2-Phenylethyl)-1*H*-imidazol-2-yl]acetamide (22)

Compound **22** was prepared from **21** and *N*-carbamimidoylacetamide (**16**) according to the same procedure used for compound **17** and was obtained as an off-white solid (10% yield). ^{1}H NMR (DMSO-d_6) δ 2.02 (3H, s), 2.67–2.74 (2H, m), 2.81–2.88 (2H, m), 6.39 (1H, s), 7.13–7.29 (5H, m), 10.97 (2H, br s); FAB MS m/e (M+H)$^+$ 230; HRMS (ESI) Calcd for $C_{13}H_{16}N_3O$ (M+H)$^+$: 230.1293, found: 230.1293.

5.1.5. 4-(2-Phenylethyl)-1*H*-imidazol-2-amine (23)

Compound **23** was prepared from **22** according to the same procedure used for compound **18** and was obtained as a pale yellow solid (93% yield). ^{1}H NMR (DMSO-d_6) δ 2.55–2.61 (2H, m), 2.77–2.83 (2H, m), 5.05 (2H, br s), 6.12 (1H, s), 7.13–7.29 (5H, m), 10.11 (1H, br s); FAB MS m/e (M+H)$^+$ 188; HRMS (ESI) Calcd for $C_{11}H_{14}N_3$ (M+H)$^+$: 188.1188, found: 188.1190.

5.1.6. A mixture of methyl 4-[(*Z*)-2-(2-acetamido-1,3-thiazol-4-yl)vinyl]benzoate and methyl 4-[(*E*)-2-(2-acetamido-1,3-thiazol-4-yl)vinyl]benzoate (26)

Potassium *tert*-butoxide (3.9 g) was added to a mixture of [4-(methoxycarbonyl)benzyl](triphenyl)phosphonium bromide (**25**) (14.3 g) and DMF (75 mL) at 0 °C under a nitrogen atmosphere. The reaction mixture was stirred at 0 °C for 15 min, and *N*-(4-formylthiazol-2-yl)acetamide (**24**)[9] (5.0 g) was then added to the mixture at 0 °C. The reaction mixture was further stirred at room temperature for 13 h and then poured into ice–H_2O. The precipitate was collected in vacuo and washed with Et_2O to give **26** (*Z*:*E* = 2:1) (7.8 g, 88%) as an off-white solid. Mp 175–177 °C; ^{1}H NMR (DMSO-d_6) δ 2.13 (3H × 2/3, s), 2.16 (3H × 1/3, s), 3.85 (3H, s), 6.61 (2H × 2/3, s), 7.05 (1H × 2/3, s), 7.26 (1H × 1/3, d, *J* = 15.5 Hz), 7.26 (1H × 1/3, s), 7.37 (1H × 1/3, d, *J* = 15.5 Hz), 7.64 (2H × 2/3, d, *J* = 8.5 Hz), 7.69 (2H × 1/3, d, *J* = 8.5 Hz), 7.90 (2H × 2/3, d, *J* = 8.5 Hz), 7.94 (2H × 1/3, d, *J* = 8.5 Hz), 12.05 (1H, br s); FAB MS *m*/*e* (M+H)$^+$ 303.

5.1.7. Methyl 4-[2-(2-acetamido-1,3-thiazol-4-yl)ethyl]benzoate (27)

A mixture of **26** (119 g), 10% palladium on carbon (118 g), AcOH (300 mL), and DMF (2000 mL) was stirred under a hydrogen atmosphere (3 atm) at room temperature for 6 h, and then filtered through a Celite® pad. The filtrate was concentrated in vacuo and the residual solid was suspended in AcOEt, and then filtered in vacuo. The filtrate was concentrated in vacuo and the obtained residue was purified by flash column chromatography over silica gel with hexane/AcOEt (1:2) to $CHCl_3$/MeOH (10:1) as an eluent and triturated with Et_2O to give **27** (69 g, 57%) as a pale yellow solid. Mp 170–171 °C; ^{1}H NMR (DMSO-d_6) δ 2.11 (3H, s), 2.86–2.95 (2H, m), 2.97–3.05 (2H, m), 3.83 (3H, s), 6.72 (1H, s), 7.35 (2H, d, *J* = 8.5 Hz), 7.87 (2H, d, *J* = 8.5 Hz), 12.08 (1H, br s); FAB MS *m*/*e* (M+H)$^+$ 305; HRMS (ESI) Calcd for $C_{15}H_{17}N_2O_3S$ (M+H)$^+$: 305.0960, found: 305.0966.

5.1.8. A mixture of {4-[(*Z*)-2-(2-acetamido-1,3-thiazol-4-yl)vinyl]phenyl}acetic acid and {4-[(*E*)-2-(2-acetamido-1,3-thiazol-4-yl)vinyl]phenyl}acetic acid (29)

Compound **29** was prepared from **24** and [4-(carboxymethyl)benzyl](triphenyl) phosphonium bromide (**28**) according to the same procedure used for compound **26** and was obtained as a white powder (*Z*:*E* = 5:1) (94% yield). ^{1}H NMR (DMSO-d_6) δ 2.12 (3H × 5/6, s), 2.15 (3H × 1/6, s), 3.52 (2H × 5/6, s), 3.54 (2H × 1/6, s), 6.46 (1H × 5/6, d, *J* = 12.5 Hz), 6.54 (1H × 5/6, d, *J* = 12.5 Hz), 6.95 (1H, s), 7.11–7.49 (6H × 1/6, m), 7.20 (2H × 5/6, d, *J* = 8.0 Hz), 7.41 (2H × 5/6, d, *J* = 8.0 Hz), 12.10 (1H, br s), 12.42 (1H, br s); FAB MS *m*/*e* (M+H)$^+$ 303.

5.1.9. Methyl (2*E*)-3-{4-[(*E*)-2-(2-acetamido-1,3-thiazol-4-yl)vinyl]phenyl}acrylate (32)

Compound **32** was prepared from methyl (2*E*)-3-(4-formylphenyl)acrylate (**30**) and [(2-acetamido-1,3-thiazol-4-yl)methyl](triphenyl)phosphonium chloride (**31**)[9] according to the same procedure used for compound **26** and was obtained as a pale yellow wax (70% yield). ^{1}H NMR (DMSO-d_6) δ 2.15 (3H, s), 3.73 (3H, s), 6.66 (1H, d, *J* = 16.0 Hz), 7.24 (1H, d, *J* = 14.5 Hz), 7.55–7.78 (2H, m), 7.95 (4H, s), 12.20 (1H, br s); FAB MS *m*/*e* (M+H)$^+$ 329; HRMS (ESI) Calcd for $C_{17}H_{17}N_2O_3S$ (M+H)$^+$: 329.0960, found: 329.0960.

5.1.10. Methyl 3-{4-[2-(2-acetamido-1,3-thiazol-4-yl)ethyl]phenyl}propanoate (33)

Compound **33** was prepared from **32** according to the same procedure used for compound **27** and was obtained as a colorless wax (76% yield). ^{1}H NMR (DMSO-d_6) δ 2.11 (3H, s), 2.60 (2H, t, *J* = 7.5 Hz), 2.80 (2H, t, *J* = 7.5 Hz), 2.89 (4H, m), 3.57 (3H, s), 6.72 (1H, s), 7.11 (4H, s), 12.06 (1H, br s); FAB MS *m*/*e* (M+H)$^+$ 333; HRMS (ESI) Calcd for $C_{17}H_{21}N_2O_3S$ (M+H)$^+$: 333.1273, found: 333.1274.

5.1.11. 4-[2-(2-Acetamido-1,3-thiazol-4-yl)ethyl]benzoic acid (34a)

To a solution of **27** (330 mg) in dioxane (3.3 mL) was added 1 M NaOH (0.43 mL) at 0 °C and then the mixture was refluxed for 2 h. Volatiles were evaporated in vacuo and the obtained residue was dissolved in H_2O and washed once with AcOEt. The aqueous layer was adjusted to pH 2 using 1 M HCl, and the resulting precipitate was collected by filtration to give **34a** (218 mg, 69%) as a colorless solid. ^{1}H NMR (DMSO-d_6) δ 2.11 (3H, s), 2.87–3.05 (4H, m), 6.73 (1H, s), 7.32 (2H, d, *J* = 8.0 Hz), 7.84 (2H, d, *J* = 8.0 Hz), 12.06 (1H, br s), 12.78 (1H, br s); FAB MS *m*/*e* (M+H)$^+$ 291; HRMS (ESI) Calcd for $C_{14}H_{15}N_2O_3S$ (M+H)$^+$: 291.0803, found: 291.0808; Anal. Calcd for $C_{14}H_{14}N_2O_3S{\cdot}0.08C_2H_4O_2$: C, 57.62; H, 4.89; N, 9.49; S, 10.86. Found: C, 58.00; H, 4.80; N, 9.23; S, 10.38.

5.1.12. {4-[2-(2-Acetamido-1,3-thiazol-4-yl)ethyl]phenyl}acetic acid (34b)

Compound **34b** was prepared from **29** according to the same procedure used for compound **27** and was obtained as an off-white solid (29% yield). ^{1}H NMR (DMSO-d_6) δ 2.11 (3H, s), 2.86–2.93 (4H, m), 3.50 (2H, s), 6.74 (1H, s), 7.14 (4H, s), 12.07 (1H, s), 12.24 (1H, br s); FAB MS *m*/*e* (M+H)$^+$ 305; HRMS (ESI) Calcd for $C_{15}H_{17}N_2O_3S$ (M+H)$^+$: 305.0960, found: 305.0962.

5.1.13. 3-{4-[2-(2-Acetamido-1,3-thiazol-4-yl)ethyl]phenyl}propanoic acid (34c)

Compound **34c** was prepared from **33** according to the same procedure used for compound **34a** and was obtained as a colorless solid (88% yield). ^{1}H NMR (DMSO-d_6) δ 2.11 (3H, s), 2.52 (2H, t, *J* = 7.5 Hz), 2.77 (2H, t, *J* = 7.5 Hz), 2.89 (4H, m), 6.73 (1H, s), 7.11 (4H, s), 12.10 (1H, br s); FAB MS *m*/*e* (M+H)$^+$ 319; HRMS (ESI) Calcd for $C_{16}H_{19}N_2O_3S$ (M+H)$^+$: 319.1116, found: 319.1122.

5.1.14. *tert*-Butyl (4-{4-[2-(2-acetamido-1,3-thiazol-4-yl)ethyl]phenyl}-1*H*-imidazol-2-yl)carbamate (36a)

To a solution of **34a** (300 mg) in CH_2Cl_2 (4.5 mL) was added dropwise oxalyl chloride (0.16 mL) at 0 °C under a nitrogen atmosphere. After stirring for 5 min, two drops of DMF were added to the reaction mixture, which was then stirred under ice-cooling for 1 h. The solvent was then evaporated to give acid chloride as a darkish yellow powder, which was then dissolved in CH_2Cl_2 (4.5 mL) and the resulting solution was cooled in an ice-bath. To the solution was added dropwise 2 M (trimethylsilyl)diazomethane/hexane (1.0 mL) at 0 °C under a nitrogen atmosphere. The reaction mixture was stirred at room temperature for 2 h, and then 4 M HCl/AcOEt (1.0 mL) and DMF (2 mL) were added at 0 °C under a nitrogen atmosphere. After stirring the solution at room temperature for 12 h, the organic solvent was removed in vacuo. The obtained halo-ketone was dissolved in DMF (6 mL) and then *tert*-butyl carbamimidoylcarbamate (**35**) (493 mg) was added to the solution at 0 °C under a nitrogen atmosphere. The reaction mixture was stirred at 65 °C for 7 h and then concentrated in vacuo. The obtained residue was purified by flash column chromatography over silica gel with $CHCl_3$/MeOH (50:1–20:1) as an eluent to give **36a** (101 mg, 23%) as an off-white solid. ^{1}H NMR (DMSO-d_6) δ 1.58 (9H, s), 2.12 (3H, s), 2.85–2.98 (4H, m), 6.55 (1H, s), 6.72 (1H, s), 7.16 (2H, d, *J* = 8.0 Hz), 7.62 (2H, d, *J* = 8.0 Hz), 8.25 (1H, br s), 12.08 (1H, br s); FAB MS *m*/*e* (M+H)$^+$ 428; HRMS (ESI) Calcd for $C_{21}H_{26}N_5O_3S$ (M+H)$^+$: 428.1756, found: 428.1760.

5.1.15. *tert*-Butyl (4-{4-[2-(2-acetamido-1,3-thiazol-4-yl)ethyl]benzyl}-1*H*-imidazol-2-yl)carbamate (36b)

Compound **36b** was prepared from **34b** and **35** according to the same procedure used for compound **36a** and was obtained as a yellow amorphous solid (22% yield). ^{1}H NMR (DMSO-d_6) δ 1.52 (9H, s), 2.11 (3H, s), 2.79–2.99 (4H, m), 3.52–3.64 (2H, m), 5.15 (1H, br s), 6.36 (1H, s), 6.49–6.59 (1H, m), 6.72 (1H, s), 7.06–7.18 (4H, m), 12.05 (1H, br s); FAB MS *m*/*e* (M+H)$^+$ 442; HRMS (ESI) Calcd for $C_{22}H_{28}N_5O_3S$ (M+H)$^+$: 442.1913, found: 442.1913.

5.1.16. *tert*-Butyl (4-{4-[2-(2-acetamido-1,3-thiazol-4-yl)ethyl]phenethyl}-1*H*-imidazol-2-yl)carbamate (36c)

Compound **36c** was prepared from **34c** and **35** according to the same procedure used for compound **36a** and was obtained as an off-white amorphous solid (26% yield). ^{1}H NMR (DMSO-d_6) δ 1.53 (9H, s), 2.11 (3H, s), 2.70–2.93 (8H, m), 6.38 (1H, s), 6.72 (1H, s), 7.10 (4H, s), 12.06 (1H, br s); FAB MS *m*/*e* (M+H)$^+$ 456; HRMS (ESI) Calcd for $C_{23}H_{30}N_5O_3S$ (M+H)$^+$: 456.2069, found: 456.2074.

5.1.17. *N*-(4-{2-[4-(2-Amino-1*H*-imidazol-4-yl)phenyl]ethyl}thiazol-2-yl)acetamide hydrochloride (37a)

A mixture of **36a** (32 mg), 4 M HCl/AcOEt (0.4 mL), and MeOH (1 mL) was stirred at room temperature for 10 h under a nitrogen atmosphere. The solvent was removed in vacuo and the residual amorphous substance was solidified with AcOEt to give **37a** (21 mg, 76%) as an off-white solid. ^{1}H NMR (DMSO-d_6) δ 2.11 (3H, s), 2.88–2.96 (4H, m), 6.50 (1H, s), 6.71 (1H, s), 7.25 (2H, d, J = 8.0 Hz), 7.55 (2H, d, J = 8.0 Hz), 9.14 (1H, br s), 12.01 (1H, br s); FAB MS *m*/*e* (M+H)$^+$ 328; HRMS (ESI) Calcd for $C_{16}H_{18}N_5OS$ (M+H)$^+$: 328.1232, found: 328.1231.

5.1.18. *N*-[4-(2-{4-[(2-Amino-1*H*-imidazol-4-yl)methyl]phenyl}ethyl)thiazol-2-yl]acetamide hydrochloride (37b)

Compound **37b** was prepared from **36b** according to the same procedure used for compound **37a** and was obtained as a pale yellow solid (74% yield). ^{1}H NMR (DMSO-d_6) δ 2.12 (3H, s), 2.77–2.96 (4H, m), 3.71–3.85 (2H, m), 6.57 (1H, s), 6.72 (1H, s), 7.078–7.21 (4H, m), 11.64 (1H, s), 12.05 (1H, s); FAB MS *m*/*e* (M+H)$^+$ 342; HRMS (ESI) Calcd for $C_{17}H_{20}N_5OS$ (M+H)$^+$: 342.1389, found: 342.1388.

5.1.19. *N*-[4-(2-{4-[(2-Amino-1*H*-imidazol-4-yl)ethyl]phenyl}ethyl)thiazol-2-yl]acetamide hydrochloride (37c)

Compound **37c** was prepared from **36c** according to the same procedure used for compound **37a** and was obtained as an off-white solid (96% yield). ^{1}H NMR (DMSO-d_6) δ 2.12 (3H, s), 2.65–2.95 (8H, m), 6.51 (1H, br s), 6.71 (1H, s), 7.12 (4H, s), 11.58 (1H, br s), 12.07 (1H, br s); FAB MS *m*/*e* (M+H)$^+$ 356; HRMS (ESI) Calcd for $C_{18}H_{22}N_5OS$ (M+H)$^+$: 356.1545, found: 356.1540; Solubility pH 5 = 197 μg/mL, pH 7 = 28 μg/mL.

5.2. Molecular modeling

5.2.1. Human VAP-1 model

A side-chain conformational search and minimization for Leu469 of the three-dimensional (3D) structure of VAP-1 with TPQ in an active conformation (PDB-code: 2C11,[11] resolution: 2.90 Å) was performed using the LowMode MD[16] function in the Molecular Operating Environment (MOE) program[17] with the MMFF94x forcefield. The bound 2-hydrazinopyridine ligand was then deleted.

5.2.2. Docking study

Compounds were docked to the human VAP-1 model using the docking program GOLD version 5.1.[18–20] The ligand-binding pocket was defined using C$^\beta$H from Leu468 as the central atom with a radius of 20 Å. The ligand was docked covalently to nitrogen atom N1 of PAQ1729 (PAQ is used PDB entry 2C11[11]) to assign TPQ and the ligand. Each ligand was docked 10 times.

5.3. Biology

5.3.1. Inhibitory effect on human and rat VAP-1 enzyme activities

Human and rat VAP-1 enzyme activities were measured using a radiochemistry enzymatic assay with ^{14}C-benzylamine (American Radiolabeled Chemicals, St. Louis, MO, USA) as a substrate.[21] An enzyme suspension prepared from Chinese Hamster Ovary (CHO) cells stably expressing human or rat VAP-1 enzyme was preincubated with the test compound in a 96-well microplate at room temperature for 30 min. The enzyme suspension was then incubated with ^{14}C-benzylamine (final concentration of 1×10^{-5} mol/L) in a final volume of 50 μL at 37 °C for 1 h. The enzymatic reaction was stopped by the addition of 2 mol/L (50 μL) citric acid. The oxidation products were extracted directly with a toluene scintillator (200 μL), and the radioactivity was measured with a scintillation spectrometer.

5.3.2. Inhibitory effect on MAO-A and MAO-B activities

MAO-A and MAO-B enzyme activities were measured using a fluorometric enzymatic assay with 5-hydroxytriptamine and benzylamine as enzyme substrates, respectively. An enzyme suspension prepared with recombinant monoamine oxidase (MAO)-A and B (Supersomes MAO A/B®, BD Gentest, MA, USA) was used in the human MAO-A and MAO-B assays. The enzymatic reaction was performed using the Amplex® Red Oxidase Assay kit (Molecular Probes). Briefly, compound **37b** and a substrate mixture containing Amplex® Red reagent were reacted at 37 °C for 1 h with the MAO-A and MAO-B enzyme suspensions. The fluorescence of the resulting mixture was measured using a fluorescent plate reader (SPECTRA Max® M2; Molecular Devices, Osaka, Japan).

5.3.3. Measurement of ocular permeability in the diabetic rats

Male Sprague–Dawley (SD) rats (6 weeks old) were purchased from Japan Charles River Laboratories (Yokohama, Japan). Following 1 week of acclimation, one group of animals was weighed and injected intraperitoneally with 65 mg/kg STZ (Sigma–Aldrich, St. Louis, MO, USA) in citrate-buffered saline. A second group underwent sham treatments with citrate-buffered saline. Two weeks after STZ injection, plasma glucose was measured from collected plasma samples. The blood glucose value was measured using a colorimetric method, and rats that showed 350 mg/dL blood glucose levels 2 weeks after STZ treatment were diagnosed with diabetes.

Compound **37b** was given daily for 2 weeks starting 2 weeks after the completion of STZ treatment. Ocular vascular permeability was examined 24 h after the date of the final administration of **37b**. Ocular permeability was evaluated based on fluorescein leakage into the vitreous 30 min after tail vein administration of 40 mg/mL/kg sodium fluorescein solution. Permeability was expressed as the intravitreal concentration/plasma concentration ratio of fluorescein. Measurement of the fluorescein was performed using a SpectraMax® fluorescent plate reader (Molecular Devices, Osaka, Japan).

5.3.4. Measurement of plasma VAP-1 activity

On the day after the last dosing with compound **37b** in STZ diabetic rats, VAP-1 activities in plasma samples collected from each group were measured using a radio-enzyme assay with ^{14}C-benzylamine as the substrate.[21] Each plasma sample was incubated with ^{14}C-benzylamine (final concentration of 1×10^{-5} mol/L) to a

final volume of 100 μL at 37 °C for 1 h. The enzymatic reaction was stopped by the addition of 2 mol/L (100 μL) citric acid, and the oxidation products were then extracted with toluene/AcOEt (500 μL). The radioactivity of the supernatant (200 μL) was then measured with 5 mL scintillation cocktail using a scintillation spectrometer.

Acknowledgements

The authors are grateful to the staff of the Division of Analytical Science Laboratories for performing elemental analysis and spectral measurements. We thank Drs. Shinya Nagashima and Shimpei Kawakami for their valuable comments and assistance in the preparation of this manuscript.

References and notes

1. Marttila-Ichihara, F.; Smith, D. J.; Stolen, C.; Yegutkin, G. G.; Elima, K.; Mercier, N.; Kiviranta, R.; Pihlavisto, M.; Alaranta, S.; Pentikäinen, U.; Pentikäinen, O.; Fülöp, F.; Jalkanen, S.; Salmi, M. *Arthritis Rheum.* **2006**, *54*, 2852.
2. Smith, D. J.; Salmi, M.; Bono, P.; Hellman, J.; Leu, T.; Jalkanen, S. *J. Exp. Med.* **1998**, *188*, 17.
3. Yu, P. H.; Wright, S.; Fan, E. H.; Lun, Z. R.; Gubisne-Harberle, D. *Biochim. Biophys. Acta* **2003**, *1647*, 193.
4. Buffoni, F.; Ignesti, G. *Mol. Genet. Metab.* **2000**, *71*, 559.
5. Yu, P. H.; Lu, L. X.; Fan, H.; Kazachkov, M.; Jiang, Z. J.; Jalkanen, S.; Stolen, C. *Am. J. Pathol.* **2006**, *168*, 718.
6. Yu, P. H.; Deng, Y. L. *Atherosclerosis* **1998**, *140*, 357.
7. O'Sullivan, J.; Unzeta, M.; Healy, J.; O'Sullivan, M. I.; Davey, G.; Tipton, K. F. *Neuro. Toxicol.* **2004**, *25*, 303.
8. Almulki, L.; Noda, K.; Nakao, S.; Hisatomi, T.; Thomas, K. L.; Hafezi-Moghadam, A. *Exp. Eye Res.* **2010**, *90*, 26.
9. Inoue, T.; Morita, M.; Tojo, T.; Yoshihara, K.; Nagashima, A.; Moritomo, A.; Ohkubo, M.; Miyake, H. *Bioorg. Med. Chem.* **2013**, *21*, 1219.
10. Jakobsson, E.; Nilsson, J.; Källström, U.; Ogg, D.; Kleywegt, G. J. *Acta Crystallogr., Sect. F: Struct. Biol. Cryst. Commun.* **2005**, *61*, 274.
11. Jakobsson, E.; Nilsson, J.; Ogg, D.; Kleywegt, G. J. *Acta Crystallogr., Sect. D: Biol. Crystallogr.* **2005**, *61*, 1550.
12. Airenne, T. T.; Nymalm, Y.; Kidron, H.; Smith, D. J.; Pihlavisto, M.; Salmi, M.; Jalkanen, S.; Johnson, M. S.; Salminen, T. A. *Protein Sci.* **1964**, *2005*, 14.
13. Nurminen, E. M.; Pihlavisto, M.; Lázár, L.; Szakonyi, Z.; Pentikäinen, U.; Fülöp, F.; Pentikäinen, O. T. *J. Med. Chem.* **2010**, *53*, 6301.
14. Nurminen, E. M.; Pihlavisto, M.; Lázár, L.; Pentikäinen, U.; Fülöp, F.; Pentikäinen, O. T. *J. Med. Chem.* **2011**, *54*, 2143.
15. Bissantz, C.; Kuhn, B.; Stahl, M. *J. Med. Chem.* **2010**, *53*, 5061.
16. Labute, P. *J. Chem. Inf. Model.* **2010**, *50*, 792.
17. MOE2012.12, Chemical Computing Group, Montreal, QC, Canada.
18. GOLD5.1, The Cambridge Crystallographic Data Centre, Cambridge, UK.
19. Jones, G.; Willett, P.; Glen, R. C. *J. Comput. Aided Mol. Des.* **1995**, *9*, 532.
20. Jones, G.; Willett, P.; Glen, R. C.; Andrew, R. L.; Robin, T. *J. Mol. Biol.* **1997**, *267*, 727.
21. Hayes, B. E.; Clarke, D. E. *Res. Commun. Chem. Pathol. Pharmacol.* **1990**, *69*, 71.